We have also examined the case of a compressive strain and found an opposite effect which results in enhancing the polarisation dependence of spectra of the field-induced refractive

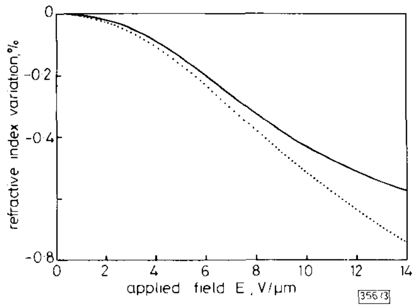

Fig. 3 *Refractive index variation as a function of applied electric field*

Strained GaAs/GaAlAs
$W = 80\,Å$
$\lambda = 0.847\,\mu m$
$\varepsilon = -0.25\%$
——— TE mode
······· TM mode

index variation. This is because of the opposite sign of the shear component of the strain further splits the light and heavy hole bands.

In conclusion, we have analysed the polarisation dependence of the field-induced refractive index variation in strained and unstrained QW structures. It is shown that the effect of strain combined with the quantum-size effect can be used to control the polarisation dependence of the refractive index variation which is significant in thin QW. The results indicate that while narrow QW structures can be useful for polarisation filtering, the application of a biaxial tensile stress to the QW can suppress such polarisation dependence and hence is useful for realising polarisation-independent electro-optic devices.

T. C. CHONG
H. W. WAN
S. J. CHUA

Centre for Optoelectronics
Department of Electrical Engineering
National University of Singapore
10 Kent Ridge Cresent, Singapore 0511

11th May 1990

References

1 WAKITA, K., YOSHIKUNI, Y., and KAWAMURA, Y.: 'Highly efficient InGaAs/InAlAs MQW waveguide phase shifter', *Electron. Lett.*, 1986, **23**, pp. 303–304

2 SAKANO, S., INOUE, H., NAKAMURA, H., KATSUYAMA, T., and MATSUMURA, H.: 'InGaAsP/InP monolithic integrated circuit with lasers and an optical switch', *Electron. Lett.*, 1986, **22**, pp. 594–596

3 YAMAMOTO, H., ASADA, M., and SUEMATSU, Y.: 'Theory of refractive index variation in quantum well structure and related intersectional optical switch', *J. Lightwave Technol.*, 1988, **LT-6**, pp. 1831–1840

4 KIKUGAWA, T., RAVIKUMAR, K. G., SHIMOMURA, K., IZUMI, A., MATSUBARA, K., MIYAMOTO, Y., ARAI, S., and SUEMATSU, Y.: 'Switching operation in OMVPE grown GaInAs/InP MQW intersectional optical switch structures', *IEEE Photon. Technol. Lett.*, 1989, **1**, pp. 126–128

5 CHONG, T. C., and FONSTAD, C. G.: 'Theoretical gain of strained-layer semiconductor lasers in the large strain regime', *IEEE J. Quantum Electron.*, 1989, **QE-25**, pp. 171–178

6 KIM, Y. S., LEE, S. S., RAMASWAMY, R. V., SAKAI, S., KAO, Y. C., and SHICHIJO, H.: 'Single mode AlGaAs/GaAs optical waveguide and phase modulator grown on Si substrates by molecular beam epitaxy'. Technical Digest, IOOC'89, vol. 1, 18D2-5, pp. 68–69

7 HENSEL, J. C., and FEHER, G.: 'Cyclotron resonance experiments in uniaxially stressed silicon: valence band inverse mass parameters and deformation potentials', *Phys. Rev.*, 1963, **129**, pp. 1041–1062

ELECTRICAL CHARACTERISATION OF THE p-TYPE DOPANT DIFFUSION OF HIGHLY DOPED AlGaAs/GaAs HETEROJUNCTION BIPOLAR TRANSISTORS GROWN BY MOCVD

Indexing terms: Doping, Diffusion

The emitter base threshold voltage is found to be a very efficient method of characterising *p*-type dopant diffusion in highly doped heterojunction bipolar transistors. Simulated curves have been successfully used to determine the amount of diffusion at different doping levels, showing the ability of MOCVD to achieve a high base doping level without any dopant diffusion.

Introduction: Very high speed performances have been demonstrated with AlGaAs/GaAs heterojunction bipolar transistors (HBTs), provided high base doping levels are used to reduce the intrinsic base resistance which is, among the parasitic elements, the most important one. Very high *p*-type doping levels were first achieved by MBE using Be[1] and more recently by CBE using C.[2] Attempts have been made to achieve such high doping levels by MOCVD either with Zn[3] or C.[4] The main problem in introducing such high doping levels in HBT structures is the control of the dopant diffusion during growth. The diffusion of dopant toward the AlGaAs emitter layer induces a drastic reduction of the DC current gain. Since the dopant diffusion increases with the doping level, the control of the diffusion is even more important in highly doped structures.

The amount of diffusion cannot be precisely determined by the current gain reduction, which is dependent on many other parameters (surface and interface recombination, electron diffusion length). The current gain is also dependent on the current density. The maximum current gain cannot therefore be measured. On large geometry devices, it is not always possible, because of parasitics effects (emitter current crowding, thermal effects) to reach the current density required for maximum DC current gain. On small geometries, the intrinsic maximum current gain is often never reached, because of the gain reduction associated with surface recombination currents. We have found that another electrical characteristic, the emitter base threshold voltage, V_{be}, is a very efficient indicator of the amount of *p*-type dopant diffusion towards the emitter layer. We present modelling demonstrating the accuracy of this characterisation and show the ability of MOCVD to realise highly doped HBT structures, without diffusion, using Zn dopant.

Modelling: Simulations have been carried out, with 1-D numerical simulation software which solves the drift-diffusion equation[5] to evaluate the influence of the characteristic parameters of the emitter-base interface on the threshold voltage. The threshold voltage is defined as the emitter-base voltage necessary to generate collector current. In this letter, it is considered at a reference current density of $110\,A/cm^2$, for which the influence of the series resistances is negligible. The basic structure is presented in Fig. 1. The emitter is an *n*-type Si-doped $Al_{0.3}Ga_{0.7}As$ layer with a doping level of $2 \times 10^{17}\,cm^{-3}$, the base is a *p*-type Zn-doped GaAs layer with a doping level of $3 \times 10^{19}\,cm^{-3}$. Between these two regions, there is a 300 Å thick *n*-type AlGaAs region, where the Al composition is decreased from 30 to 0%. The collector is an *n*-type Si doped GaAs layer with a doping level of $2 \times 10^{16}\,cm^{-3}$. We have investigated the influence of several parameters on the threshold voltage: the emitter and base doping levels, the thickness of the gradual region and the amount of diffusion in the gradual region.

The influence of the *n*-type and *p*-type doping levels was investigated first (Fig. 1). The emitter doping level has no influence on the threshold voltage at the chosen current density. On the contrary, the influence of the base doping level can be detected, a variation of the doping level from $2 \times 10^{18}\,cm^{-3}$ to $3 \times 10^{19}\,cm^{-3}$ induces a variation of 55 mV.

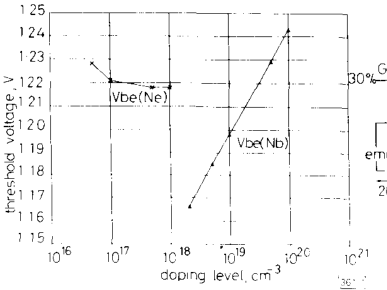

Fig. 1 *Characteristics of threshold voltage*

× emitter doping variation: base doping $3 \times 10^{19}\,cm^{-3}$
▲ base doping variation: emitter doping $2 \times 10^{17}\,cm^{-3}$

Since the control by MOCVD of the doping level is better than 10%, the base doping level will be a controlled source of threshold voltage variation. The base sheet resistance value deduced from TLM measurements allows the assessment of the doping level value.

The influence of the gradual region thickness on the threshold voltage is more significant. A variation of the gradual region thickness from 0 to 200 Å induces a variation of the threshold voltage from 1·37 to 1·22 V. When the gradual region is larger than 200 Å, the variation of the threshold voltage is very small. Considering the fact that the thickness control is better than 2% and that the gradual region thickness is optimised at 300 Å, this parameter will not be responsible for threshold voltage variations.

The *p*-type dopant diffusion, simulated with a simple exponential model, towards the emitter layer is the most significant parameter (Fig. 2). For a *p*-type doping level of

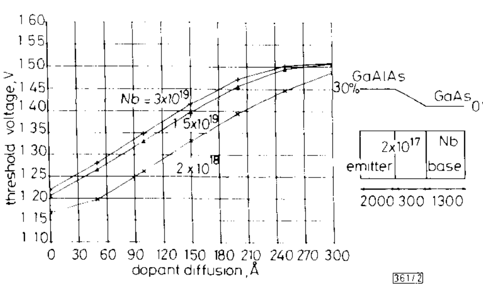

Fig. 2 *Dependence of threshold voltage on p-type diffusion*

× $2 \times 10^{18}\,cm^{-3}$
▲ $1{\cdot}5 \times 10^{19}\,cm^{-3}$
+ $3 \times 10^{19}\,cm^{-3}$

$3 \times 10^{19}\,cm^{-3}$, without any dopant diffusion, the threshold voltage is 1·22 V. A light diffusion of 100 Å induces a threshold voltage of 1·35 V. When the diffusion reaches 300 Å, the threshold voltage is 1·50 V. The threshold voltage is then very sensitive to dopant diffusion. When the diffusion is deeper than 300 Å, there is no more variation of the threshold voltage. When the diffusion is more important than the thickness of the gradual region, there is a drastic decrease of the current gain.

These simulations have shown that the *p*-type dopant diffusion is the only significant parameter in the threshold voltage variation. With the simulated curves, the threshold voltage can then be used as a very precise indicator of the amount of *p*-type dopant diffusion.

Experimental procedure: Transistors were fabricated with a simple double mesa fabrication technology. Five wafers grown by MOCVD with the same epitaxial structure, except the base doping level and thickness have been processed. The first one is a reference wafer with a base doping level of $2 \times 10^{18}\,cm^{-3}$, for which the dopant diffusion is very limited. The other wafers present base doping levels higher than $10^{19}\,cm^{-3}$, sample 2 was grown under non-optimised growth conditions, while samples 3, 4 and 5 were grown under optimised conditions.[6]

Electrical characterisation: TLM measurements performed on the wafers allow the calculation of the sheet base resistance. The measured values are presented in Table 1. The value measured on wafer 3 is among the lowest ever achieved by MOCVD. The DC current gains have also been measured, the values indicate dopant diffusion less than 300 Å. The measured threshold voltages are presented in Table 1, as well as the base sheet resistance, the DC current gain and the dopant diffusion deduced from SIMS measurements.

The threshold voltages deduced from wafers 1 and 5 are in good agreement with the results of the simulation with no dopant diffusion, showing the increase of the threshold voltage with the base doping level. The simulated and measured values are 1·17 V for a base doping level of $2 \times 10^{18}\,cm^{-3}$ and 1·22 V for $3 \times 10^{19}\,cm^{-3}$. The threshold voltages measured on wafers 2–5 allow the calculation of the amount of dopant diffusion from the simulated curve (Fig. 2). Wafer 2 grown under non-optimised conditions is then credited with a dopant diffusion of 145 Å. Wafers 3, 4 and 5 grown under optimised conditions are credited with 55 Å, 40 Å and 0 Å, respectively, for doping levels varying between 1·5 and $3 \times 10^{19}\,cm^{-3}$. These values are more reliable than values deduced from SIMS analysis. Values deduced from SIMS can be erroneous, considering the depth resolution, and can only be considered as indicative of an order of magnitude. The values of the DC current gain demonstrate the ambiguity of the relation between the gain and the amount of dopant diffusion. The increase of current gain between wafers 2 and 5 is related to the base thickness and to a reduction of dopant diffusion. The decrease of gain between wafers 4 and 3 is chiefly related to an increase of recombination for sample 4, the dopant diffusion being similar.

These results show the ability of MOCVD to grow HBT structures, with high base doping level using Zn. *p*-type doping levels as high as $3 \times 10^{19}\,cm^{-3}$ can be obtained, leading to low base sheet resistance (250 Ω/□). *p*-type dopant diffusion can be avoided, which is demonstrated by the value of the threshold voltage (1·22 V) related to a good value of the maximum current gain (50).

Conclusion: We have demonstrated that for heterojunction bipolar transistors, the emitter-base threshold voltage is directly related to the *p*-type dopant diffusion towards the emitter layer. Simulated and measured values have been compared and the simulated curves have been used to successfully deduce the amount of diffusion, in the case of highly doped structures.

This study has also shown the ability of MOCVD to realise HBTs with a high base doping level using Zn dopant, without *p*-type dopant diffusion.

Table 1 ELECTRICAL CHARACTERISTICS OF WAFERS

wafer	N_A (cm^{-3}) (SIMS)	R_B (Ω/□)	β (110 A/cm^2)	β (max)	V_{be} (V)	diffusion (Å V_{be}) this study	diffusion (Å) (SIMS)
1	2×10^{18}	1200	400	500	1·17	0	ud
2	3×10^{19}	180	15	15	1·41	145	360
3	$1{\cdot}5 \times 10^{19}$	420	60	100	1·27	55	280
4	$1{\cdot}5 \times 10^{19}$	300	30	35	1·25	40	400
5	3×10^{19}	250	35	50	1·22	0	ud

Acknowledgments: The authors will like to thank L. Dugrand for epitaxial growth; A. M. Duchenois, P. Launay, P. Berdaguer and M. Riet for device processing; Y. Gao for SIMS measurements; J. F. Palmier for providing the physical data; and M. Bon, A. Scavennec and E. Caquot for fruitful discussions.

J. DANGLA
C. DUBON-CHEVALLIER
M. FILOCHE
R. AZOULAY

Centre National d'Etudes des Télécommunications
Laboratoire de Bagneux
196 avenue Henri-Ravera, 92220 Bagneux, France

14th May 1990

References

1 LIÉVIN, J. L., DUBON-CHEVALLIER, C., ALEXANDRE, F., LEROUX, G., DANGLA, J., and ANKRI, D.: '$Ga_{0.72}Al_{0.28}As/Ga_{0.99}Be_{0.01}As$ heterojunction bipolar transistor grown by molecular beam epitaxy', *IEEE Electron. Dev. Lett.*, 1986, **EDL-7**, pp. 129–131
2 SAITO, K., TOKUMITSU, E., AKATSUKA, T., MIYAUCHI, M., YAMADA, T., KONAGAI, M., and TAKAHASHI, K.: 'Characterisation of *p*-type GaAs heavily doped with carbon grown by metallorganic MBE'. *Inst. Phys. Conf. Ser.*, 1988, **96**, pp. 69–72
3 ENQUIST, P. B., HUTCHBY, J. A., CHANG, M. F., ASBECK, P. M., SHENG, N. H., and HIGGINS, J. A.: 'High frequency performance of MOVPE *npn* AlGaAs/GaAs heterojunction bipolar transistors', *Electron. Lett.*, 1989, **25**, pp. 1124–1125
4 CUNNINGHAM, B. T., STILLMAN, G. E., and JACKSON, G. S.: 'Carbon-doped base GaAs/AlGaAs heterojunction bipolar transistor grown by metalorganic chemical vapor deposition using carbon tetrachloride as a dopant source', *Appl. Phys. Lett.*, 1990, **56**, (4), pp. 361–363
5 PALMIER, J. F., DANGLA, J., CAQUOT, E., and CAMPANA, M.: 'Numerical simulation of electrical transport in III-V microstructure devices'. Proc. Nasecode IV, Boole Press, Dublin, 1985
6 AZOULAY, R., DUGRAND, L., GAO, Y., DANGLA, J., DUBON-CHEVALLIER, C., and RIET, M.: to be published in *Appl. Phys. Lett.*

IMPROVED DESIGN OF MINIMUM-PHASE FIR DIGITAL FILTERS BY CEPSTRUM AND FAST HARTLEY TRANSFORM

Indexing terms: Filters, Transforms

An equiripple minimum-phase FIR filter is designed using the cepstrum and the fast Hartley transform (FHT). This fast procedure is performed entirely in the real domain and requires only two short-length FHT computations. This method avoids complicated phase wrapping and greatly reduces the aliasing error.

Introduction: Minimum phase FIR filters have certain practical advantages, e.g., minimum group delay, reduced order for given gain specification and lower coefficient sensitivity,[1] when compared with the linear phase FIR filters. They are highly attractive in some applications, such as CTD transversal filters and communication channel filters.

Herrman and Schuessler[2] have developed a method for transforming equiripple linear-phase designs into equiripple minimum-phase designs with half the order and with a magnitude response equal to the square root of the prototype. A numerial root-finding procedure is required for this method. Main and Nainer[3] proposed a design procedure to overcome this difficulty by using homomorphic deconvolution. However, a complicated phase wrapping algorithm is required in the computation. Pei and Lu[4] introduced a differential cepstrum design avoiding the need for phase wrapping. However, differential cepstrum has the aliasing problem[5] and requires three larger-length FFT's in order to implement it. Reddy[6] has recently used the cepstrum computed from the spectral log magnitude function to overcome the aliasing problem. The procedure requires only two FFT computations and avoids the processing of phase. In that letter, the fast Hartley transform (FHT) is introduced to design equiripple minimum phase FIR filters through cepstrum. This fast procedure only needs two real FHT computations, and avoids the complicated phase wrapping and polynomial root-finding algorithms. The aliasing error is also greatly reduced.

Minimum phase filter design: According to Herrman and Schuessler's method,[2] the relationship between linear phase $H(z)$, second-order zeros $H_1(z)$ and minimum phase $H_2(z)$ is as follows:

$$
\begin{aligned}
H_1(z) &= H(z) + \delta_2 z^{-(N-1)/2} \\
H_1(z) &= z^{-(N-1)/2} H_2(z) H_2(z^{-1}) \\
H_2(e^{j\omega}) &= \sqrt{[H_1(e^{j\omega})]}
\end{aligned} \tag{1}
$$

where N and δ_2 are the length and the stopband ripple of the linear phase filter $H(z)$.

Let $\hat{h}_1(n)$ and $\hat{h}_2(n)$ be the complex cepstrum of the filters $H_1(z)$ and $H_2(z)$, respectively. The relation between $\hat{h}_2(n)$ and $\hat{h}_1(n)$ is[3]

$$\hat{h}_2(n) = \tfrac{1}{2}[\hat{h}_1(n) + \hat{h}_1(-n)] = c_1(n) \qquad n > 0 \tag{2}$$

$c_1(n)$ corresponds to the cepstrum of $H_1(z)$ and is defined as

$$\ln |H_1(e^{j\omega})| = \sum_{n=-\infty}^{\infty} c_1(n) e^{-j\omega n} \tag{3}$$

Once $\hat{h}_2(n)$ is computed using eqns. 2 and 3, the minimum phase filter impulse response $h_2(n)$ can be obtained from its complex cepstrum $\hat{h}_2(n)$.[3]

$$h_2(n) = \hat{h}_2(n)h_2(0) + \sum_{k=0}^{n-1} \frac{k}{n} \hat{h}_2(n) h_2(n-k) \qquad 0 \le n \le (N-1)/2 \tag{4}$$

Then the equiripple minimum-phase filters can be designed using only the magnitude function of the linear phase filter, thereby avoiding the processing of the phase. The complex cepstrum $\hat{h}_2(n)$ decays at least as fast as $1/n$, and its corresponding differential cepstrum[4] $\hat{h}_{d2}(n+1) = n\hat{h}_2(n)$ does not decay with an envelope of $1/n$. This approach can greatly reduce the aliasing error by using the cepstrum instead of the differential cepstrum.

The fast Hartley transform[7–9] has recently been considered as an interesting alternative to the FFT, we can use the real FHT here to calculate the log magnitude response and the cepstrum of the filter $H_1(z)$ very efficiently.

The discrete Fourier and Hartley transform of $x(n)$ are defined as

$$\mathrm{DFT}: X(k) = \sum_{n=0}^{N-1} x(n) e^{-j2\pi nk/N} \tag{5a}$$

$$\mathrm{DHT}: H_x(k) = \sum_{n=0}^{N-1} x(n) \operatorname{cas}\left(\frac{2nk}{N}\pi\right) \tag{5b}$$

where $\operatorname{cas}(x) = \sin(x) + \cos(x)$. The inverse relation is

$$\mathrm{IDFT}: x(n) = \frac{1}{N} \sum_{k=0}^{N-1} X(k) e^{j2\pi nk/N} \tag{6a}$$

$$\mathrm{IDHT}: x(n) = \frac{1}{N} \sum_{k=0}^{N-1} H_x(k) \operatorname{cas}\left(\frac{2nk}{N}\pi\right) \tag{6b}$$

The relation of the DHT and DFT of a real sequence $x(n)$ is

$$
\begin{aligned}
\mathrm{Even}\,[H_x(k)] &= [H_x(k) + H_x(-k)]/2 \\
&= \mathrm{Re}\,[X(k)]
\end{aligned} \tag{7a}
$$

$$
\begin{aligned}
\mathrm{Odd}\,[H_x(k)] &= [H_x(k) - H_x(-k)]/2 \\
&= -\mathrm{Im}\,[X(k)]
\end{aligned} \tag{7b}
$$